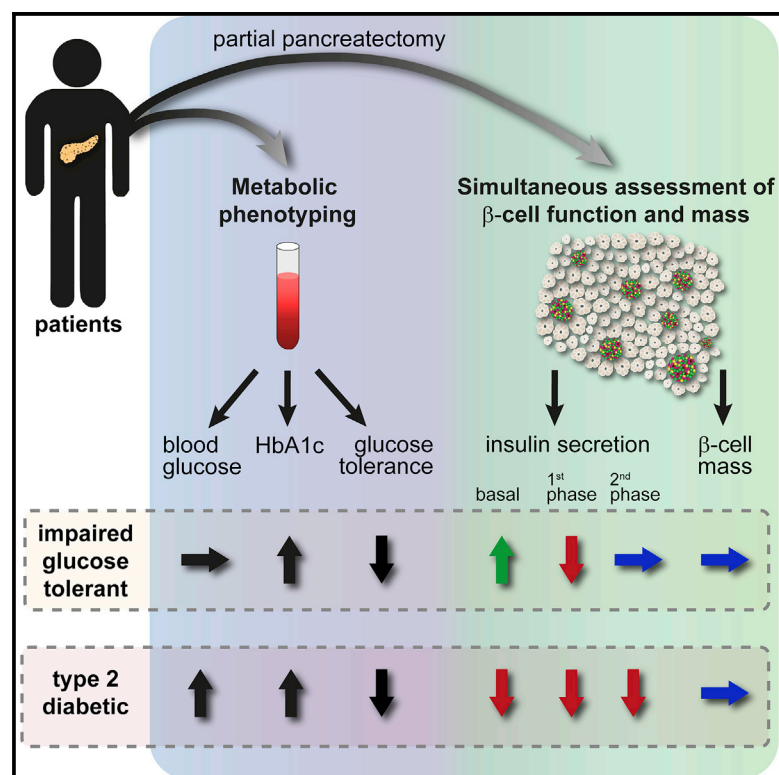


Cell Reports

Dysfunction of Persisting β Cells Is a Key Feature of Early Type 2 Diabetes Pathogenesis

Graphical Abstract



Authors

Christian M. Cohrs, Julia K. Panzer, Denise M. Drotar, ..., Jürgen Weitz, Michele Solimena, Stephan Speier

Correspondence

stephan.speier@tu-dresden.de

In Brief

Cohrs et al. utilize pancreas tissue slices of metabolically phenotyped subjects undergoing pancreatectomy to assess β cell pathogenesis in type 2 diabetes development. They reveal β cell dysfunction as an early hallmark in type 2 diabetes pathogenesis, manifesting as increased basal and missing first-phase insulin secretion, although β cell mass is maintained.

Highlights

- Pancreas tissue slices from surgical resections allow study of β cells in T2D
- β cell dysfunction develops early and deteriorates further in T2D pathogenesis
- Basal and first-phase insulin is altered in impaired glucose-tolerant donor tissue
- β cell mass in tissue slices appears intact throughout the progression to T2D



Dysfunction of Persisting β Cells Is a Key Feature of Early Type 2 Diabetes Pathogenesis

Christian M. Cohrs,^{1,2,3,9} Julia K. Panzer,^{1,2,3,9} Denise M. Drotar,^{1,2,3} Stephen J. Enos,^{1,2,3} Nicole Kipke,^{3,4} Chunguang Chen,^{1,2,3} Robert Bozsak,^{1,2,3} Eyke Schöniger,^{1,3,4} Florian Ehehalt,⁵ Marius Distler,⁵ Ana Brennand,⁶ Stefan R. Bornstein,^{6,7} Jürgen Weitz,^{1,5} Michele Solimena,^{1,3,4,8} and Stephan Speier^{1,2,3,10,*}

¹Paul Langerhans Institute Dresden (PLID) of the Helmholtz Zentrum München at the University Clinic Carl Gustav Carus of Technische Universität Dresden, Helmholtz Zentrum München, Neuherberg, Germany

²Institute of Physiology, Faculty of Medicine, Technische Universität Dresden, Dresden, Germany

³German Center for Diabetes Research (DZD), München-Neuherberg, Germany

⁴Molecular Diabetology, Faculty of Medicine, Technische Universität Dresden, Dresden, Germany

⁵Department of GI-, Thoracic- and Vascular Surgery, University Hospital Carl Gustav Carus, Technische Universität Dresden, Dresden, Germany

⁶Department of Diabetes, School of Life Science & Medicine, Faculty of Life Sciences & Medicine, King's College London, London, UK

⁷Department of Medicine III, University Hospital Carl Gustav Carus, Dresden, Germany

⁸Max Planck Institute of Molecular Cell Biology and Genetics, Dresden, Germany

⁹These authors contributed equally

¹⁰Lead Contact

*Correspondence: stephan.speier@tu-dresden.de

<https://doi.org/10.1016/j.celrep.2020.03.033>

SUMMARY

Type 2 diabetes is characterized by peripheral insulin resistance and insufficient insulin release from pancreatic islet β cells. However, the role and sequence of β cell dysfunction and mass loss for reduced insulin levels in type 2 diabetes pathogenesis are unclear. Here, we exploit freshly explanted pancreas specimens from metabolically phenotyped surgical patients using an *in situ* tissue slice technology. This approach allows assessment of β cell volume and function within pancreas samples of metabolically stratified individuals. We show that, in tissue of pre-diabetic, impaired glucose-tolerant subjects, β cell volume is unchanged, but function significantly deteriorates, exhibiting increased basal release and loss of first-phase insulin secretion. In individuals with type 2 diabetes, function within the sustained β cell volume further declines. These results indicate that dysfunction of persisting β cells is a key factor in the early development and progression of type 2 diabetes, representing a major target for diabetes prevention and therapy.

INTRODUCTION

Type 2 diabetes is a metabolic disorder that causes hyperglycemia in patients and affects hundreds of millions of people worldwide. It is responsible for debilitating long-term complications, decreased quality of life, and premature death. Unfortunately, present treatment options are unable to adequately control hyperglycemia and prevent the negative impact of type 2 diabetes. Development of effective therapeutic approaches to correct

inadequate insulin levels in response to elevated blood glucose relies on targeting the correct underlying pathological mechanism. However, it is still under debate whether and at which stage of diabetes pathogenesis insulin insufficiency is the result of compromised β cell function (i.e., the amount of insulin released by each individual β cell), reduced β cell mass (i.e., the number of β cells within the pancreas), and/or a combination of both (Li et al., 2019; Taylor et al., 2019; Weir, 2020). It has been suggested that β cell mass loss already happens in the early stage of diabetes before β cell functional impairment (Weir, 2020; Weir and Bonner-Weir, 2004, 2013) and that β cell mass deficit actually predisposes an organism to impaired glucose homeostasis in diabetes (Costes et al., 2013; Leahy, 2005; Taylor et al., 2019). On the other hand, by examining the timing and relationship between changes in blood glucose, β cell volume, and insulin secretion, arguments have been made that the functional deficit is more dominant and is requisite for the development of type 2 diabetes (Ferrannini, 2010; Kahn et al., 2006, 2009; Ritzel et al., 2006; Saisho, 2014). Hence, it is unclear whether and when the objective in type 2 diabetes prevention and therapy should be to protect and restore β cell function, i.e., the amount of insulin released by each individual β cell, or to prevent the death of β cells and increase their mass (Chen et al., 2017; Halban et al., 2014). A main reason for the inability to address these key questions is the lack of samples and technologies to simultaneously assess β cell function and mass. Systemic metabolic tests *in vivo* cannot reliably distinguish between the contribution of number and function of β cells to plasma insulin levels. At present, β cell mass in humans can only be assessed by histology of pancreatic specimens from organ donors or surgical patients, which do not allow functional testing. Utilizing this approach, studies have reported a wide range of β cell mass reduction in subjects with type 2 diabetes, stretching from 24% to 65% (Butler et al., 2003; Clark et al., 1988; Inaishi et al., 2016; Rahier et al., 2008; Sakuraba et al., 2002; Yoon et al., 2003), whereas others



suggested this method to overestimate β cell loss in type 2 diabetes (Marselli et al., 2014). In either case, an additional substantial loss of function in the residual β cells seems imperative to explain the extreme reduction in insulin response found in type 2 diabetes (Ferrannini et al., 2005; Gastaldelli et al., 2004; Holman, 1998; Jensen et al., 2002; Osei et al., 1997; Ward et al., 1984). Most importantly, current data do not elucidate to which extent these two distinct components contribute to type 2 diabetes pathogenesis and whether loss of β cell mass and/or function is cause or consequence of the uncontrolled hyperglycemia. Only limited and conflicting data are available on β cell mass in pre-diabetes or impaired glucose-tolerant subjects (Butler et al., 2003; Meier et al., 2009). Consequently, the role of β cell mass and function in the development of type 2 diabetes and their importance for prevention and therapy have been controversially discussed (Clark et al., 2001; DeFronzo et al., 2013; Henquin et al., 2008; Meier and Bonadonna, 2013; Weir and Bonner-Weir, 2013).

Here, we employed a novel approach of human pancreas tissue slices in combination with a unique collection of fresh pancreas tissue samples from metabolically phenotyped subjects to simultaneously assess β cell volume and function within pancreatic tissue. Thereby, we provide direct evidence that dysfunction of persisting β cells is an early feature of type 2 diabetes pathogenesis that remains an important mechanism throughout disease progression.

RESULTS

Pancreas Tissue Slices of Metabolically Phenotyped Subjects Allow Assessment of β Cell Volume and Function in Type 2 Diabetes Pathogenesis

To explore the detailed 3D cellular morphology and insulin secretion of intact human pancreatic tissue under near physiological conditions, we utilized the pancreas tissue slice technique (Marciniak et al., 2013, 2014; Speier and Rupnik, 2003) in freshly explanted surgical samples from subjects who underwent pancreatectomy (Ehehalt et al., 2015; Sturm et al., 2013). These subjects, 4 non-diabetic (ND), 4 having impaired glucose tolerance (IGT), and 6 type 2 diabetes (Table S1), were part of a larger cohort of 61 ND, 71 IGT, and 88 type 2 diabetes subjects (Figure 1), in which patients in the days immediately prior to surgery had been metabolically phenotyped based on their clinical history, HbA1c (Figure 1A), fasting blood glucose (fBG) levels (Figure 1B), and an oral glucose tolerance test (OGTT) (Figure 1C) for being either ND or having IGT or type 2 diabetes, according to the American Diabetes Association (ADA) guidelines (Solimena et al., 2018). Within this cohort, the mean age was slightly increased in IGT and type 2 diabetes subjects in comparison to ND (Figure 1D), whereas body mass index (BMI) (Figure 1E) and HOMA2-IR (Figure 1F) did not differ among the three groups. Fasting C-peptide levels (Figure 1G) were significantly decreased, and fasting proinsulin (Figure 1H) significantly increased in type 2 diabetes. As a result, the insulin/proinsulin ratio was significantly decreased in IGT and type 2 diabetes in comparison to ND (Figure 1I). Consequently, HOMA2-%B, as an indicator of insulin release, was significantly different between all groups of the cohort (Figure 1J). Tissue samples obtained immediately after surgery of the subjects

providing tissue for this study were further processed by vibratome sectioning to obtain 120- μ m-thick tissue slices with a dimension of ca. 3 \times 3 mm (Figure 1K). Only viable tissue slices displaying a limited number of dead cells were used for subsequent assays (Figure S1).

Islet Cell Morphology and Volume Are Not Altered in Pancreas Tissue Slices of IGT and Type 2 Diabetes Subjects

Endocrine cell content was quantified by 3D morphometry of the entire slice volume for the three main endocrine cell types at cellular resolution (Figures 2A–2C). Applying this procedure, we could quantify the endocrine fraction and cellular distribution within a given volume of pancreatic tissue (Figure S2). We found that, in ND subjects, endocrine cells constituted $0.48\% \pm 0.09\%$ of pancreas volume (Figure 2D). This was slightly less than the fractional area previously reported from histological studies (Butler et al., 2010; Wang et al., 2013). This difference is probably related to differences in the experimental and analysis approach used for the measurement of cell volumes within tissue pieces in comparison to the assessment of cell area in thin sections. Moreover, tissue used in our study mainly originated from the pancreas head, which has been reported to contain fewer islets than the rest of the pancreas (Reers et al., 2009; Saito et al., 1978). Interestingly, endocrine cell volume was not significantly changed being $1.06\% \pm 0.33\%$ and $0.91\% \pm 0.60\%$ (Figure 2D), respectively. Similarly, distinct endocrine cell volume fractions of β , α , and δ cells were not significantly altered in pancreas of ND, IGT, and type 2 diabetes subjects (Figures 2E–2G). In addition, the mean diameter of all detected endocrine objects, which refers to all hormone-positive-stained cells identified as single cells (1 cell; volume of 500–1,000 μm^3), small clusters (2–10 cells; volume of 1,001–10,000 μm^3), or islets (>10 cells; volume >10,000 μm^3), of up to >250 μm diameter as well as their density in the pancreatic tissue were comparable between the groups (Figures 2H and 2I). Furthermore, our analysis demonstrated that the vast majority of endocrine objects in the human pancreas, $82.02\% \pm 3.13\%$, were individual cells or small clusters of up to 10 endocrine cells scattered throughout the exocrine tissue (Figures 2J and 2K). However, these single cells and small clusters only contributed $18.10\% \pm 4.22\%$ to the overall volume of endocrine cells (Figures 2L and 2M). The vast majority of the endocrine volume was comprised by islets with ≥ 11 cells (Figures 2L and 2M). Neither the distribution of endocrine object size nor their contribution to total endocrine volume was significantly changed in the pancreas of IGT or type 2 diabetes subjects (Figures 2H–2M). Thus, detailed 3D morphometry of endocrine cell volume, composition, and distribution within the studied human pancreatic tissue revealed no difference between ND, IGT, and type 2 diabetes subjects.

β Cell Function Is Compromised in Pancreas of IGT Subjects and Deteriorates in Type 2 Diabetes

Utilizing the unique potential of pancreas tissue slices, we additionally assessed β cell function by measuring kinetic insulin secretion. Upon perfusion, pancreas tissue slices from ND subjects showed a typical bi-phasic insulin secretory pattern in response to elevated glucose levels exhibiting a peak in insulin

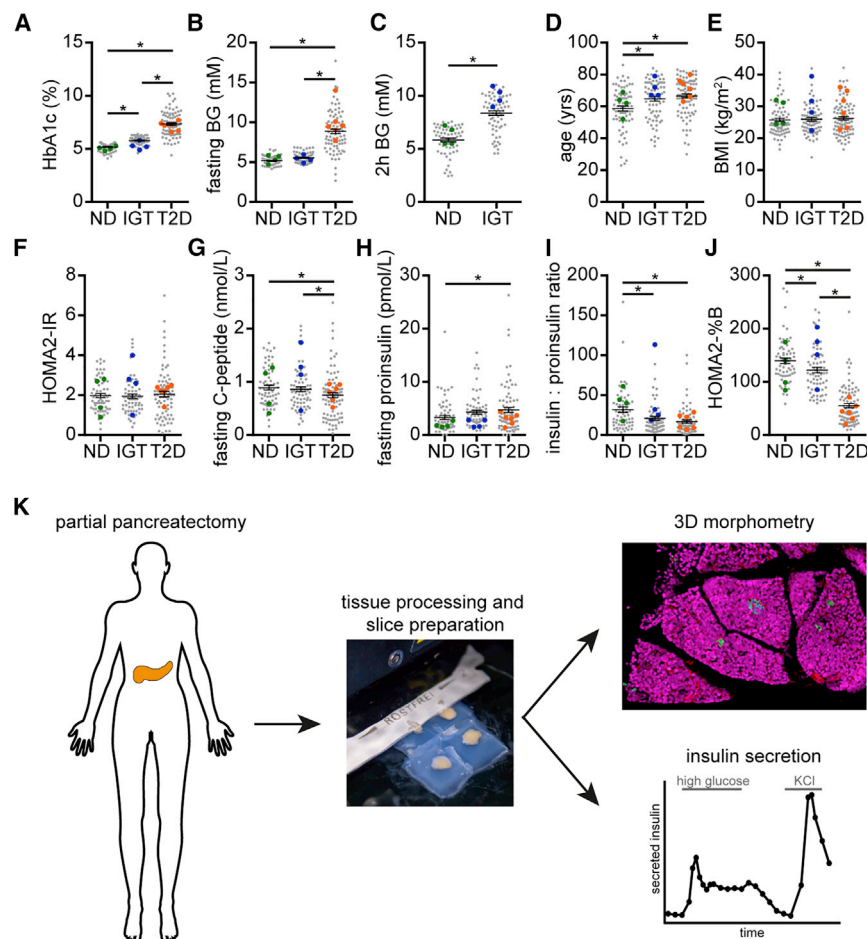


Figure 1. Experimental Approach and Clinical Data

(A–C) Parameters used to classify individual patients prior to surgery into the different disease groups according to ADA criteria with (A) plasma HbA1c, (B) plasma fasting blood glucose, and (C) plasma 2-h blood glucose value during an OGTT. (D–J) Age (D) and BMI values (E) of patients within the entire cohort as well as (F) HOMA2-IR, (G) fasting serum C-peptide, (H) fasting serum proinsulin, (I) insulin: proinsulin ratio, and (J) β cell functional index. (F) and (J) were calculated with the HOMA2 model calculator (<https://www.dtu.ox.ac.uk/homacalculator/>).

(K) Schematic overview of the experimental workflow with human patients undergoing partial pancreatectomy after being metabolically phenotyped (A–J). During partial pancreatectomy surgery, pancreas tissue is resected and non-cancerous tissue is procured and further processed for tissue slice preparation. Viable tissue slices are subsequently used for fixation and 3D morphometric analysis or subjected to kinetic insulin secretion.

Gray dots in (A)–(J) represent single patients with $n = 62$ (non-diabetic [ND]), $n = 71$ (impaired glucose tolerant [IGT]), and $n = 88$ (type 2 diabetes [T2D]). Lines show mean \pm SEM. Colored dots (ND $n = 4$; IGT $n = 4$; T2D $n = 6$) represent patients used in the current study. Statistical analysis was performed on the entire cohort by one-way ANOVA and post hoc comparison of disease groups with Sidak's correction for multiple comparisons. * $p < 0.05$.

See also Table S1.

secretion during the first phase, followed by a second-phase plateau (Figures 3A and S3A). Intriguingly, tissue slices from IGT subjects showed a significantly increased basal insulin secretion, although glucose-stimulated insulin release was comparable to ND (Figures 3A–3C and S3A). In contrast, the baseline insulin secretion of slices from type 2 diabetes patients was similar to that of slices from ND subjects and significantly lower compared to IGT (Figures 3A–3C and S3A). Moreover, slices from both IGT and type 2 diabetes subjects lacked the typical first-phase peak prior to the second-phase plateau (Figures 3A–3C and S3A). When expressed as stimulation index to illustrate the stimulatory potential of glucose over baseline, slices from ND subjects displayed 5-fold increased insulin secretion during first phase and 3-fold elevated secretion during the second phase (Figures 3D and S3B), comparable to the response observed from islets isolated from ND organ donors (Figure S4). In contrast, samples from IGT and type 2 diabetes subjects showed a severely diminished stimulation index leading to a significantly reduced area under the curve of insulin secretion in first and second phase (Figures 3D–3F and S3B). Insulin content, in particular when normalized to β cell volume measured in adjacent slices of the respective patient (see Figure 2), was strongly reduced in tissue slices ob-

tained from type 2 diabetes subjects (Figures 3G and 3H), indicating emptying of insulin granule stores. Consequently, the insulin secreted from slices of IGT and type 2 diabetes was increased when expressed as a fraction of their insulin content (Figures 3I and S3C).

Clinical Parameters of Type 2 Diabetes Pathogenesis Are Associated with the Functional Decline of β Cells

Furthermore, our approach allowed us to compare β cell function and volume in pancreas tissue slices directly with various clinical parameters from the same subjects (Figures 4 and S5). We found that endocrine cell volume in tissue slices correlated linearly with age (Figure 4A) of the tissue donors, independent of their status of glucose homeostasis. However, there was no significant correlation between endocrine cell mass and BMI (Figure 4B), HbA1c (Figure 4C), or fasting glucose (Figure 4D). Stimulated insulin secretion from tissue slices showed no correlation with age (Figure 4E) or BMI (Figure 4F) of the donor. Interestingly, when assessing the relationship of stimulated insulin secretion and HbA1c (Figure 4G) and fasting glucose (Figure 4H), ND, IGT, and type 2 diabetes subjects clustered in groups, indicating an association of β cell function with clinical parameters of type 2 diabetes pathogenesis.

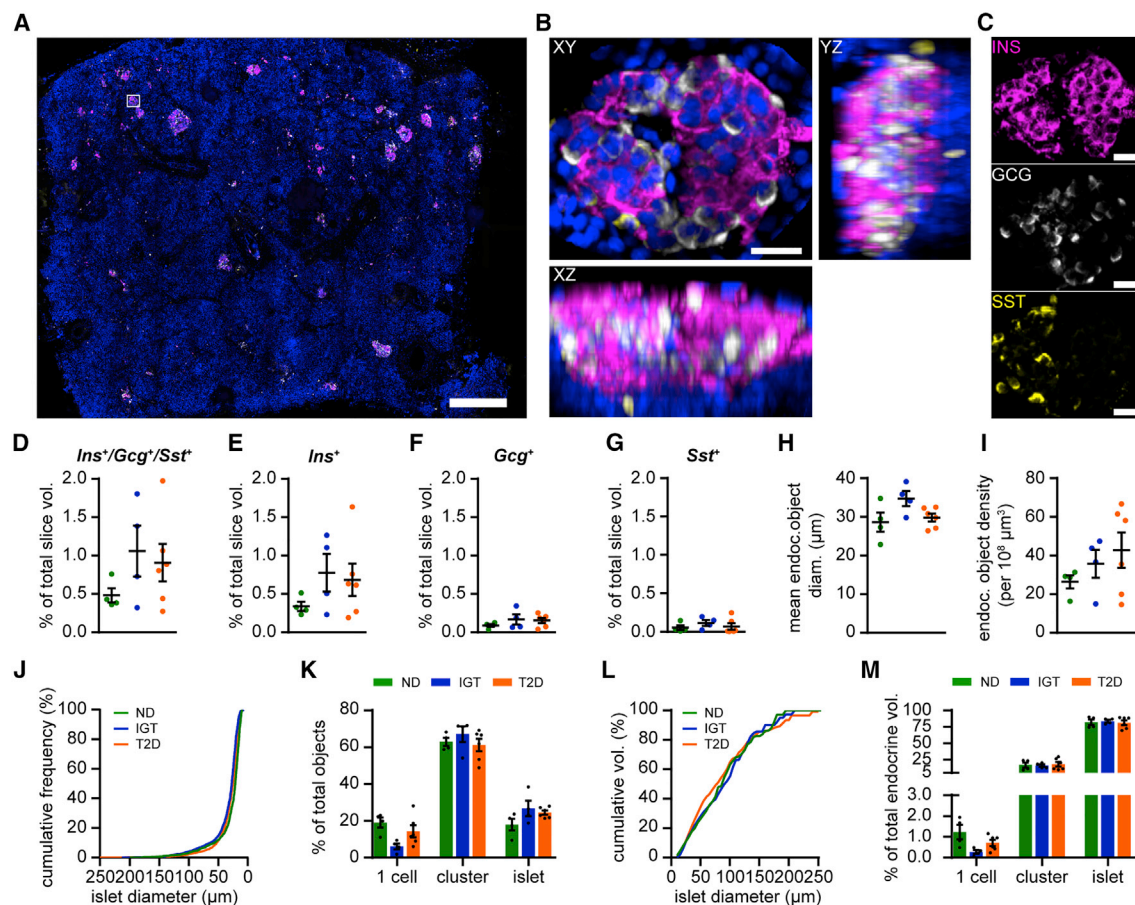


Figure 2. 3D Histomorphometric Analysis of Human Pancreas Tissue Slices

(A) Maximum intensity projection of an entire human pancreas tissue slice stained with antibodies against insulin (magenta), glucagon (grey), and somatostatin (yellow) counterstained with DAPI (blue). Scale bar, 500 μ m.

(B) Magnified maximum intensity projection of a single islet (boxed in A) with insulin (magenta), glucagon (grey), somatostatin (yellow), and DAPI (blue) in XY (upper left), XZ (bottom left), and YZ (upper right) orientation. Scale bar, 50 μ m.

(C) Maximum intensity projection of the same islet as in (B) for single hormone staining for insulin (magenta), glucagon (grey), and somatostatin (yellow). Scale bars, 50 μ m.

(D–G) Quantification of hormone-positive volumes as percent of the total slice volumes of ND (green), IGT (blue), and T2D (orange) samples for (D) Ins+/Gcg+/Sst+ volume, (E) Ins+ volume, (F) Gcg+ volume, and (G) Sst+ volume.

(H and I) Mean endocrine object diameter (H) and endocrine object density (I) of the individual samples from ND, IGT, and T2D patients.

(J and K) Frequency distribution of hormone-positive endocrine objects by diameter (J) and mean percent of endocrine objects (K) grouped by appearance of single cells, cluster (up to 10 cells), and islets (>11 cells) for individual samples from ND, IGT, and T2D specimens.

(L and M) Cumulative volume of all endocrine objects by diameter (L) and mean contribution (M) of single cells (up to 10 cells), and islets (>11 cells) to the entire endocrine (Ins+/Gcg+/Sst+) volume from individual ND, IGT, and T2D samples. ND n = 4, IGT n = 4, and T2D n = 6 with data presented as mean \pm SEM. See also Figure S2.

DISCUSSION

Our data demonstrate that β cells exhibit significant functional deterioration and exhaustion already at early stages of type 2 diabetes pathogenesis, at which subjects exhibit impaired glucose tolerance but are not yet diabetic. Conversely, β cell volume is maintained at this stage of disease progression, which is in line with the previous finding of unchanged β cell mass in impaired glucose-tolerant subjects (Meier et al., 2009). Thus, our results identify β cell dysfunction as an initial feature of diabetes development and not necessarily as consequence of a

preceding loss in β cell mass. Interestingly, in non-diabetic subjects with more elevated levels of fasting blood glucose (>110 mg/dL) β cell mass was reported to be decreased (Butler et al., 2003). This suggests that non-diabetic individuals with significantly elevated fasting blood glucose might experience advanced disease progression or a different etiology of diabetes pathogenesis in comparison to individuals in pre-diabetic subjects with impaired glucose tolerance (Rizza, 2010). Our study shows that functional decline of β cells emerges in pancreatic tissue of IGT individuals and manifests as increased basal insulin release, a known feature of impaired glucose homeostasis

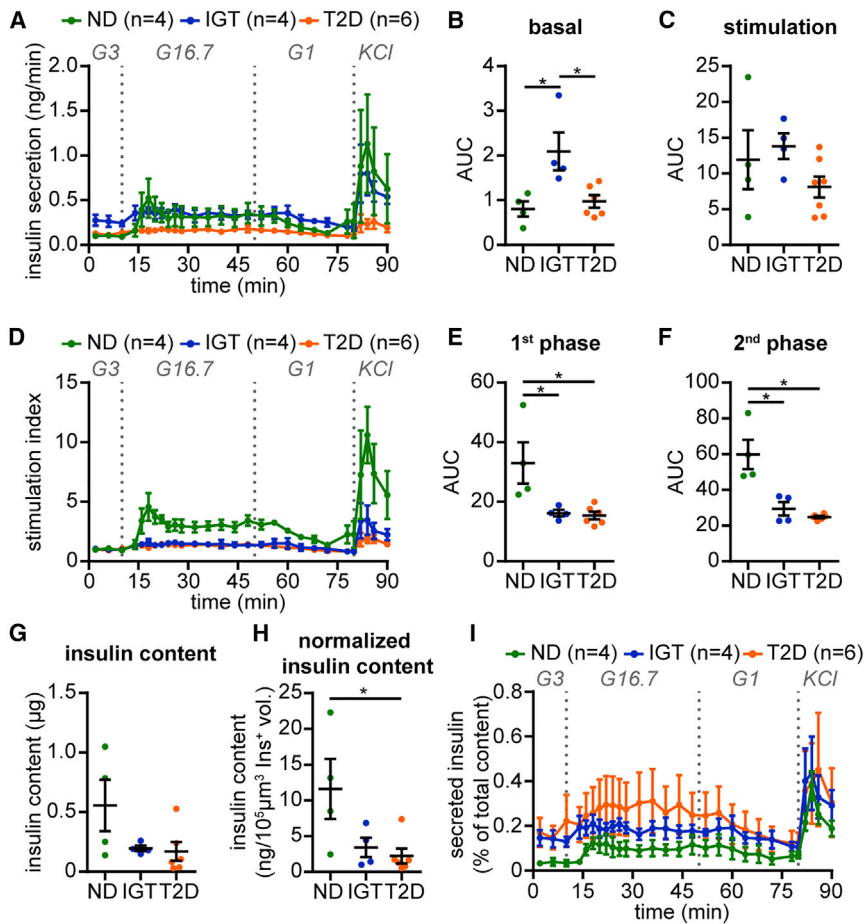


Figure 3. Assessment of β Cell Function *In Situ*

(A) Insulin secretion of slices from ND (green), IGT (blue), and T2D (orange) subjects presented as absolute secretion in ng/min. G1, KRBH buffer containing 1 mM glucose; G3, KRBH buffer containing 3 mM glucose; G16.7mM, KRBH buffer with 16.7 mM glucose; KCl, KRBH buffer with 16.7 mM glucose and 60 mM KCl (final concentration [f.c.]). (B and C) Area under the curve (AUC) measurements of data in (A) for (B) basal secretion (minutes 0–10) and (C) entire stimulation period (minutes 10–50) of the individual samples.

(D) Insulin secretory pattern of ND (green), IGT (blue), and T2D (orange) pancreas tissue slices during perfusion expressed as fold increase to basal secretion within the first 10 min (3 mM glucose).

(E and F) AUC measurements of data presented in (D) for (E) first-phase insulin secretion (minutes 10–22) and (F) second-phase insulin secretion (minutes 28–48) of single samples.

(G) Slice insulin content after perfusion of ND, IGT, and T2D specimens.

(H) Slice insulin content normalized to Ins+ volume assessed in adjacent slices for the respective subject (see also Figure 2).

(I) Insulin secretory pattern of ND (green), IGT (blue), and T2D (orange) pancreas tissue slices during perfusion expressed as % of total content. ND $n = 4$, IGT $n = 4$, and T2D $n = 6$ with data presented as mean \pm SEM.

All data in this figure are analyzed using one-way ANOVA with post hoc comparison of disease groups using Sidak's correction for multiple comparisons. * $p < 0.05$.

See also Figures S3 and S4.

observed in individuals with IGT and with predictive value for type 2 diabetes development (Charles et al., 1991). Yet we show here that elevated basal insulin secretion appears without a significant increase in peripheral insulin resistance and occurs *ex vivo* in the absence of a direct systemic influence (Weyer et al., 2000). Additionally, β cells from IGT subjects exhibited a loss of first-phase insulin release, confirming the early manifestation of this feature of dysregulated insulin release, previously observed in IGT subjects *in vivo* in response to an OGTT (Gerich, 1997). Similar to elevated basal insulin release, our data demonstrated that also the loss of first-phase insulin secretion from pancreatic tissue was the result of β cell dysfunction of an unchanged β cell volume. Thus, although insulin dysregulation has been shown to occur in early stages of type 2 diabetes development (Abdul-Ghani et al., 2006; DeFronzo et al., 2013; Ferrannini et al., 2005), our study provides further insight into underlying mechanisms by demonstrating an intrinsic β cell defect without concurrent changes in β cell mass and independent of systemic insulin resistance. Notably, recent transcriptomic analysis of pancreatic surgical samples from subjects within this and a similar cohort detected no significant transcriptomic changes in laser-capture microdissected islets of individuals with IGT but only in those from patients with overt type 2 diabetes (Gerst et al., 2018; Solimena et al., 2018). This indicates that early β cell dysfunction in

IGT subjects is not the consequence of alterations in gene expression but most likely in the levels of other factors, such as proteins, lipids, carbohydrates, or metabolites. In subjects with type 2 diabetes, the first phase of insulin release remained absent, indicating ongoing β cell dysfunction. Moreover, the basal and second phase of insulin release from pancreas tissue slices declined in individuals with type 2 diabetes in comparison to IGT, potentially as a result of long-lasting β cell stress, progressing β cell dysfunction, and β cell exhaustion. Intriguingly, in our study, pancreatic tissue obtained from type 2 diabetes subjects showed no decrease in β cell volume. This is in contrast to findings of several histological studies on the pancreas from type 2 diabetes organ donors (Butler et al., 2003; Clark et al., 1988; Inaishi et al., 2016; Rahier et al., 2008; Sakuraba et al., 2002; Yoon et al., 2003). Discrepancies concerning β cell mass among studies can be related to variables like tissue sampling, processing and analysis, or donor and disease characteristics, including BMI, age, insulin resistance, glucose tolerance, and fasting blood glucose levels. In addition, in some studies, β cell mass might have been underestimated due to the presence of degranulated and therefore insulin-negative β cells (Marselli et al., 2014). Although the staining and imaging protocols used in our study limit the risk of underestimation of β cell mass, we cannot exclude escaping of a limited number of fully

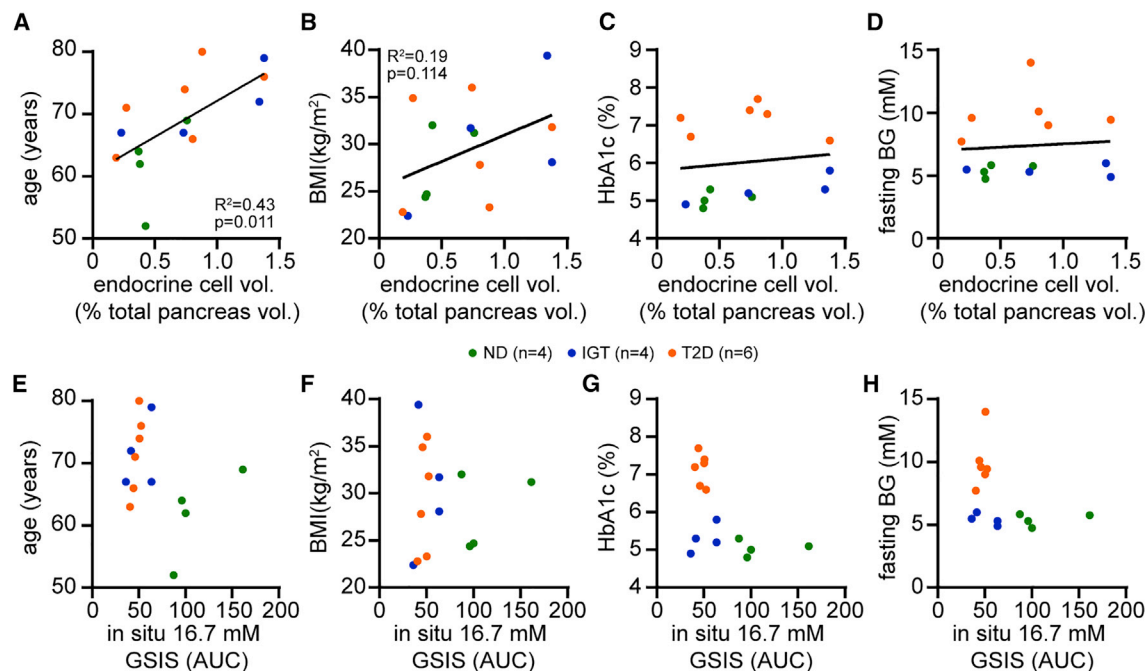


Figure 4. Association of Clinical Parameters with β Cell Function and Mass

(A–D) Regression analysis of endocrine cell volume (see Figure 2D) to (A) age, (B) BMI, (C) HbA1c, and (D) fasting blood glucose.

(E–H) Regression analysis of AUC values from insulin secretion (stimulation index) during stimulating conditions with 16.7 mM glucose (see Figure 3B) to (E) age, (F) BMI, (G) HbA1c, and (H) fasting blood glucose. ND (green) $n = 4$; IGT (blue) $n = 4$; T2D (orange) $n = 6$.

See also Figure S5.

degranulated β cells. However, a potential underestimation of β cell mass in IGT and type 2 diabetes would further strengthen our observation that β cell function and not mass is declined in slices of these patient groups. Given the strong overlap of reported β cell mass ranges in type 2 diabetes and non-diabetic individuals (Rahier et al., 2008), additional studies will be necessary to verify the sustained β cell volume found in the here studied cohort and samples. Nevertheless, our results clearly demonstrate that, even at full-blown type 2 diabetes, there are significant numbers of dysfunctional β cells present, which potentially can be functionally recovered by appropriate therapies, e.g., via the removal of potential systemic causes for β cell dysfunction and allowing restoration of secretory capacity.

When assessing the impact of our study and its relevance for the understanding of type 2 diabetes pathogenesis, specific considerations have to be made. First, due to the complexity of the protocol, we could only obtain and investigate fresh and viable pancreas tissue slices from a limited number of surgical donors. Thus, given the observed heterogeneity of pancreas and diabetes pathogenesis in humans, studies with larger populations will be necessary to confirm the general applicability of our findings. Nevertheless, the here applied direct correlation of detailed systemic metabolic parameters with organ cell morphology and function in the same individual facilitated the detection of pathogenic phenotypes as never possible before. In doing so, our data provide further insight into a controversially discussed aspect of type 2 diabetes pathogenesis. Second, subjects in our cohort underwent pancreatectomy mostly due

to a localized tumor. An effect of the neighboring tumor on the here-studied healthy tissue cannot be fully excluded, albeit pathology examination did neither reveal infiltration of cancer cells in the islets nor signs of insulinitis. Moreover, a previous study on samples from this cohort did not detect any effect of the present tumor on islet cell gene transcription in the healthy tissue (Solimena et al., 2018). Furthermore, no relationship between different cancer types and islet biology was observed in this or the previous study. Most importantly, in the vast majority of cases in which diabetes is associated with pancreatic cancer, diabetes has been shown to manifest concomitantly or less than 2 years prior to cancer diagnosis (Gullo et al., 1994; Pannala et al., 2008). In contrast, subjects included in our study had either no or long-standing diabetes (3, 6, 10, 15, 17, and 20 years duration), implicating no connection between the state of glucose homeostasis and the cancer. To avoid assessing tumor-related β cell changes, subjects with recent onset diabetes were not included in our study. Therefore, we are confident that our results reflect physiological and pathophysiological processes underlying type 2 diabetes development. Third, in our study, the pancreas tissue samples were mostly derived from the head of the pancreas. Our conclusions on the performance of each pancreas are therefore limited to this respective area and cannot exclude different developments in a different part of the pancreas. This could be relevant, as islet composition and density differ between the posterior part of the head and the tail of the pancreas (Gersell et al., 1979; Saito et al., 1978). Interestingly, islets in the pancreas head have been suggested to be

preferentially affected in metabolically challenging and pathological conditions (Ellenbroek et al., 2017; Savari et al., 2013; Wang et al., 2013). However, these considerations do not affect our conclusion of β cell dysfunction, manifesting as increased basal and loss of stimulated first-phase insulin secretion in persisting β cells, being an early crucial feature in the development of type 2 diabetes. Whether this is primarily occurring in islets in the head of the pancreas or also in the body and tail will need to be addressed in future studies. Finally, our cohort mainly consists of type 2 diabetes patients of relatively older age and with only moderate metabolic derangements, having no significant changes in fasting insulin levels or HOMA2-IR compared to ND subjects. Based on these clinical characteristics, our findings may not be directly transferable to all type 2 diabetes patients without additional studies. However, a recent study on almost 9,000 patients, which led to stratification of adult-onset diabetes patients into five different subgroups, showed that patients exhibiting rather modest metabolic alterations (defined as MARD for mild-age-related diabetes), similar to the subjects in our cohort, represent the largest patient group of adult-onset diabetes (Ahlqvist et al., 2018), further stressing the importance of our findings. Within future studies, it will be interesting to investigate whether our here-described mechanism of type 2 diabetes pathogenesis also applies to the pancreas of type 2 diabetes subgroups with different metabolic characteristics.

In conclusion, using the combination of an *in situ* tissue technology and acute human pancreas specimens of metabolically phenotyped subjects, we demonstrate that deteriorated function of β cells plays a crucial role at initial stages of type 2 diabetes development and persists throughout disease progression. We show that dysregulated insulin release, in the form of increased basal and loss of first-phase secretion, manifests at a pre-diabetic IGT state as result of β cell dysfunction within a sustained β cell volume. Thus, our results provide experimental evidence for a unique and unparalleled depiction of the pathogenesis of human type 2 diabetes, highlighting β cell dysfunction as a critical target for the development of successful diabetes prevention and therapy.

STAR★METHODS

Detailed methods are provided in the online version of this paper and include the following:

- KEY RESOURCES TABLE
- LEAD CONTACT AND MATERIALS AVAILABILITY
- EXPERIMENTAL MODEL AND SUBJECT DETAILS
- METHOD DETAILS
 - Tissue Procurement, Processing and Slicing
 - Tissue Viability
 - Perfusion
 - Immunofluorescent staining
 - Imaging and Analysis
 - Tile-Scan Analysis
- QUANTIFICATION AND STATISTICAL ANALYSIS
 - Statistical Analyses and Calculations
- DATA AND CODE AVAILABILITY

SUPPLEMENTAL INFORMATION

Supplemental Information can be found online at <https://doi.org/10.1016/j.celrep.2020.03.033>.

ACKNOWLEDGMENTS

We would like to thank Katharina Hüttner, Alin Jurisch, and Angela Hartke for excellent technical assistance; Daniela Richter, Manuela Kleeberg, Robert Grutzmann, and Gustavo Baretton for help in the provision of human pancreatic tissues; and Andreas Müller for discussion of imaging data. This work was supported with funds from the Paul Langerhans Institute Dresden (PLID) of Helmholtz Zentrum München at the University Clinic Carl Gustav Carus of Technische Universität Dresden; the German Ministry for Education and Research (BMBF) to the German Centre for Diabetes Research (DZD); the DFG—SFB/Transregio 127; the DFG—IRTG 2251; the DFG—Research Center for Regenerative Therapies Dresden, Cluster of Excellence (CRTD); and the European Foundation for the Study of Diabetes (EFSD)/Boehringer Ingelheim Basic Research Programme. Moreover, the work leading to this project has received funding from the Innovative Medicines Initiative 2 Joint Undertaking under grant agreements nos. 155005 (IMIDIA), 115881 (RHAPSODY), and 115797 (INNODIA), which include financial contributions from European Union's Seventh Framework Programme (FP7/2007-2013), Horizon 2020 research and innovation programme, and EFPIA. This work is also supported by the Swiss State Secretariat for Education, Research and Innovation (SERI) under contract number 16.0097.

AUTHOR CONTRIBUTIONS

C.M.C., J.K.P., and S.S. conceived and designed the experiments; C.M.C., J.K.P., D.M.D., S.J.E., and R.B. prepared tissue slices, performed experiments, and analyzed data; and N.K., E.S., F.E., M.D., J.W., and M.S. provided human pancreas samples and metabolic phenotyping. A.B. and S.R.B. provided human isolated islets. C.M.C., J.K.P., D.M.D., S.J.E., C.C., M.S., and S.S. analyzed the results and prepared the manuscript. S.S. is the guarantor of this work and, as such, had full access to all the data in the study and takes responsibility for the integrity of the data and the accuracy of the data analysis.

DECLARATION OF INTERESTS

The authors declare no competing interests.

Received: October 5, 2019

Revised: February 3, 2020

Accepted: March 12, 2020

Published: April 7, 2020

REFERENCES

- Abdul-Ghani, M.A., Tripathy, D., and DeFronzo, R.A. (2006). Contributions of beta-cell dysfunction and insulin resistance to the pathogenesis of impaired glucose tolerance and impaired fasting glucose. *Diabetes Care* 29, 1130–1139.
- Ahlqvist, E., Storm, P., Kärjämäki, A., Martinell, M., Dorkhan, M., Carlsson, A., Vikman, P., Prasad, R.B., Aly, D.M., Almgren, P., et al. (2018). Novel subgroups of adult-onset diabetes and their association with outcomes: a data-driven cluster analysis of six variables. *Lancet Diabetes Endocrinol.* 6, 361–369.
- Butler, A.E., Janson, J., Bonner-Weir, S., Ritzel, R., Rizza, R.A., and Butler, P.C. (2003). Beta-cell deficit and increased beta-cell apoptosis in humans with type 2 diabetes. *Diabetes* 52, 102–110.
- Butler, A.E., Cao-Minh, L., Galasso, R., Rizza, R.A., Corradin, A., Cobelli, C., and Butler, P.C. (2010). Adaptive changes in pancreatic beta cell fractional area and beta cell turnover in human pregnancy. *Diabetologia* 53, 2167–2176.
- Charles, M.A., Fontbonne, A., Thibault, N., Warnet, J.M., Rosselin, G.E., and Eschwege, E. (1991). Risk factors for NIDDM in white population. Paris prospective study. *Diabetes* 40, 796–799.

- Chen, C., Cohrs, C.M., Stertman, J., Bozsak, R., and Speier, S. (2017). Human beta cell mass and function in diabetes: Recent advances in knowledge and technologies to understand disease pathogenesis. *Mol. Metab.* 6, 943–957.
- Clark, A., Wells, C.A., Buley, I.D., Cruickshank, J.K., Vanhegan, R.I., Matthews, D.R., Cooper, G.J., Holman, R.R., and Turner, R.C. (1988). Islet amyloid, increased A-cells, reduced B-cells and exocrine fibrosis: quantitative changes in the pancreas in type 2 diabetes. *Diabetes Res.* 9, 151–159.
- Clark, A., Jones, L.C., de Koning, E., Hansen, B.C., and Matthews, D.R. (2001). Decreased insulin secretion in type 2 diabetes: a problem of cellular mass or function? *Diabetes* 50 (Suppl 1), S169–S171.
- Costes, S., Langen, R., Gurlo, T., Matveyenko, A.V., and Butler, P.C. (2013). β -cell failure in type 2 diabetes: a case of asking too much of too few? *Diabetes* 62, 327–335.
- DeFronzo, R.A., Eldor, R., and Abdul-Ghani, M. (2013). Pathophysiologic approach to therapy in patients with newly diagnosed type 2 diabetes. *Diabetes Care* 36 (Suppl 2), S127–S138.
- Ehehalt, F., Sturm, D., Rösler, M., Distler, M., Weitz, J., Kersting, S., Ludwig, B., Schwanebeck, U., Saeger, H.D., Solimena, M., and Grützmann, R. (2015). Blood glucose homeostasis in the course of partial pancreatectomy—evidence for surgically reversible diabetes induced by cholestasis. *PLoS ONE* 10, e0134140.
- Ellenbroek, J.H., Töns, H.A.M., Hanegraaf, M.A.J., Rabelink, T.J., Engelse, M.A., Carlotti, F., and de Koning, E.J.P. (2017). Pancreatic α -cell mass in obesity. *Diabetes Obes. Metab.* 19, 1810–1813.
- Ferrannini, E. (2010). The stunned beta cell: a brief history. *Cell Metab.* 11, 349–352.
- Ferrannini, E., Gastaldelli, A., Miyazaki, Y., Matsuda, M., Mari, A., and DeFronzo, R.A. (2005). beta-cell function in subjects spanning the range from normal glucose tolerance to overt diabetes: a new analysis. *J. Clin. Endocrinol. Metab.* 90, 493–500.
- Gastaldelli, A., Ferrannini, E., Miyazaki, Y., Matsuda, M., and DeFronzo, R.A.; San Antonio metabolism study (2004). Beta-cell dysfunction and glucose intolerance: results from the San Antonio metabolism (SAM) study. *Diabetologia* 47, 31–39.
- Gerich, J.E. (1997). Metabolic abnormalities in impaired glucose tolerance. *Metabolism* 46 (12, Suppl 1), 40–43.
- Gersell, D.J., Gingerich, R.L., and Greider, M.H. (1979). Regional distribution and concentration of pancreatic polypeptide in the human and canine pancreas. *Diabetes* 28, 11–15.
- Gerst, F., Jaghutriz, B.A., Staiger, H., Schulte, A.M., Lorza-Gil, E., Kaiser, G., Panse, M., Haug, S., Heni, M., Schütz, M., et al. (2018). The expression of aldolase B in islets is negatively associated with insulin secretion in humans. *J. Clin. Endocrinol. Metab.* 103, 4373–4383.
- Gullo, L., Pezzilli, R., and Morselli-Labate, A.M.; Italian Pancreatic Cancer Study Group (1994). Diabetes and the risk of pancreatic cancer. *N. Engl. J. Med.* 331, 81–84.
- Halban, P.A., Polonsky, K.S., Bowden, D.W., Hawkins, M.A., Ling, C., Mather, K.J., Powers, A.C., Rhodes, C.J., Sussel, L., and Weir, G.C. (2014). β -cell failure in type 2 diabetes: postulated mechanisms and prospects for prevention and treatment. *Diabetes Care* 37, 1751–1758.
- Henquin, J.C., Cerasi, E., Efendic, S., Steiner, D.F., and Boitard, C. (2008). Pancreatic beta-cell mass or beta-cell function? That is the question!. *Diabetes Obes. Metab.* 10 (Suppl 4), 1–4.
- Holman, R.R. (1998). Assessing the potential for alpha-glucosidase inhibitors in prediabetic states. *Diabetes Res. Clin. Pract.* 40 (Suppl), S21–S25.
- Inaishi, J., Saisho, Y., Sato, S., Kou, K., Murakami, R., Watanabe, Y., Kitago, M., Kitagawa, Y., Yamada, T., and Itoh, H. (2016). Effects of obesity and diabetes on α - and β -cell mass in surgically resected human pancreas. *J. Clin. Endocrinol. Metab.* 101, 2874–2882.
- Jensen, C.C., Cnop, M., Hull, R.L., Fujimoto, W.Y., and Kahn, S.E.; American Diabetes Association GENNID Study Group (2002). Beta-cell function is a major contributor to oral glucose tolerance in high-risk relatives of four ethnic groups in the U.S. *Diabetes* 51, 2170–2178.
- Kahn, S.E., Hull, R.L., and Utzschneider, K.M. (2006). Mechanisms linking obesity to insulin resistance and type 2 diabetes. *Nature* 444, 840–846.
- Kahn, S.E., Zraika, S., Utzschneider, K.M., and Hull, R.L. (2009). The beta cell lesion in type 2 diabetes: there has to be a primary functional abnormality. *Diabetologia* 52, 1003–1012.
- Leahy, J.L. (2005). Pathogenesis of type 2 diabetes mellitus. *Arch. Med. Res.* 36, 197–209.
- Legland, D., Arganda-Carreras, I., and Andrey, P. (2016). MorphoLibJ: integrated library and plugins for mathematical morphology with ImageJ. *Bioinformatics* 32, 3532–3534.
- Li, L., Krznar, P., Erban, A., Agazzi, A., Martin-Levilain, J., Supale, S., Kopka, J., Zamboni, N., and Maechler, P. (2019). Metabolomics identifies a biomarker revealing in vivo loss of functional β -cell mass before diabetes onset. *Diabetes* 68, 2272–2286.
- Marciniak, A., Selck, C., Friedrich, B., and Speier, S. (2013). Mouse pancreas tissue slice culture facilitates long-term studies of exocrine and endocrine cell physiology in situ. *PLoS ONE* 8, e78706.
- Marciniak, A., Cohrs, C.M., Tsata, V., Chouinard, J.A., Selck, C., Stertman, J., Reichelt, S., Rose, T., Ehehalt, F., Weitz, J., et al. (2014). Using pancreas tissue slices for in situ studies of islet of Langerhans and acinar cell biology. *Nat. Protoc.* 9, 2809–2822.
- Marselli, L., Suleiman, M., Masini, M., Campani, D., Bugliani, M., Syed, F., Martino, L., Focosi, D., Scatena, F., Olimpico, F., et al. (2014). Are we overestimating the loss of beta cells in type 2 diabetes? *Diabetologia* 57, 362–365.
- Meier, J.J., and Bonadonna, R.C. (2013). Role of reduced β -cell mass versus impaired β -cell function in the pathogenesis of type 2 diabetes. *Diabetes Care* 36 (Suppl 2), S113–S119.
- Meier, J.J., Menge, B.A., Breuer, T.G., Müller, C.A., Tannapfel, A., Uhl, W., Schmidt, W.E., and Schrader, H. (2009). Functional assessment of pancreatic beta-cell area in humans. *Diabetes* 58, 1595–1603.
- Osei, K., Gaillard, T., and Schuster, D.P. (1997). Pathogenetic mechanisms of impaired glucose tolerance and type II diabetes in African-Americans. The significance of insulin secretion, insulin sensitivity, and glucose effectiveness. *Diabetes Care* 20, 396–404.
- Pannala, R., Leirness, J.B., Bamlet, W.R., Basu, A., Petersen, G.M., and Chari, S.T. (2008). Prevalence and clinical profile of pancreatic cancer-associated diabetes mellitus. *Gastroenterology* 134, 981–987.
- Preibisch, S., Saalfeld, S., and Tomancak, P. (2009). Globally optimal stitching of tiled 3D microscopic image acquisitions. *Bioinformatics* 25, 1463–1465.
- Rahier, J., Guiot, Y., Goebbels, R.M., Sempoux, C., and Henquin, J.C. (2008). Pancreatic beta-cell mass in European subjects with type 2 diabetes. *Diabetes Obes. Metab.* 10 (Suppl 4), 32–42.
- Reers, C., Erbel, S., Esposito, I., Schmied, B., Büchler, M.W., Nawroth, P.P., and Ritzel, R.A. (2009). Impaired islet turnover in human donor pancreata with aging. *Eur. J. Endocrinol.* 160, 185–191.
- Ritzel, R.A., Butler, A.E., Rizza, R.A., Veldhuis, J.D., and Butler, P.C. (2006). Relationship between beta-cell mass and fasting blood glucose concentration in humans. *Diabetes Care* 29, 717–718.
- Rizza, R.A. (2010). Pathogenesis of fasting and postprandial hyperglycemia in type 2 diabetes: implications for therapy. *Diabetes* 59, 2697–2707.
- Saisho, Y. (2014). Importance of beta cell function for the treatment of type 2 diabetes. *J. Clin. Med.* 3, 923–943.
- Saito, K., Iwama, N., and Takahashi, T. (1978). Morphometrical analysis on topographical difference in size distribution, number and volume of islets in the human pancreas. *Tohoku J. Exp. Med.* 124, 177–186.
- Sakuraba, H., Mizukami, H., Yagihashi, N., Wada, R., Hanyu, C., and Yagihashi, S. (2002). Reduced beta-cell mass and expression of oxidative stress-related DNA damage in the islet of Japanese type II diabetic patients. *Diabetologia* 45, 85–96.

- Savari, O., Zielinski, M.C., Wang, X., Misawa, R., Millis, J.M., Witkowski, P., and Hara, M. (2013). Distinct function of the head region of human pancreas in the pathogenesis of diabetes. *Islets* 5, 226–228.
- Schindelin, J., Arganda-Carreras, I., Frise, E., Kaynig, V., Longair, M., Pietzsch, T., Preibisch, S., Rueden, C., Saalfeld, S., Schmid, B., et al. (2012). Fiji: an open-source platform for biological-image analysis. *Nat. Methods* 9, 676–682.
- Solimena, M., Schulte, A.M., Marselli, L., Ehehalt, F., Richter, D., Kleeberg, M., Mziaut, H., Knoch, K.P., Parnis, J., Bugliani, M., et al. (2018). Systems biology of the IMIDIA biobank from organ donors and pancreatectomised patients defines a novel transcriptomic signature of islets from individuals with type 2 diabetes. *Diabetologia* 61, 641–657.
- Speier, S., and Rupnik, M. (2003). A novel approach to in situ characterization of pancreatic beta-cells. *Pflugers Arch.* 446, 553–558.
- Sturm, D., Marselli, L., Ehehalt, F., Richter, D., Distler, M., Kersting, S., Grützmann, R., Bokvist, K., Froguel, P., Liechti, R., et al. (2013). Improved protocol for laser microdissection of human pancreatic islets from surgical specimens. *J. Vis. Exp.* (71), 50231.
- Taylor, R., Al-Mrabeh, A., and Sattar, N. (2019). Understanding the mechanisms of reversal of type 2 diabetes. *Lancet Diabetes Endocrinol.* 7, 726–736.
- Wang, X., Misawa, R., Zielinski, M.C., Cowen, P., Jo, J., Periwal, V., Ricordi, C., Khan, A., Szust, J., Shen, J., et al. (2013). Regional differences in islet distribution in the human pancreas—preferential beta-cell loss in the head region in patients with type 2 diabetes. *PLoS ONE* 8, e67454.
- Ward, W.K., Bolgiano, D.C., McKnight, B., Halter, J.B., and Porte, D., Jr. (1984). Diminished B cell secretory capacity in patients with noninsulin-dependent diabetes mellitus. *J. Clin. Invest.* 74, 1318–1328.
- Weir, G.C. (2020). Glucolipotoxicity, β -cells, and diabetes: the emperor has no clothes. *Diabetes* 69, 273–278.
- Weir, G.C., and Bonner-Weir, S. (2004). Five stages of evolving beta-cell dysfunction during progression to diabetes. *Diabetes* 53 (Suppl 3), S16–S21.
- Weir, G.C., and Bonner-Weir, S. (2013). Islet β cell mass in diabetes and how it relates to function, birth, and death. *Ann. N Y Acad. Sci.* 1281, 92–105.
- Weyer, C., Hanson, R.L., Tataranni, P.A., Bogardus, C., and Pratley, R.E. (2000). A high fasting plasma insulin concentration predicts type 2 diabetes independent of insulin resistance: evidence for a pathogenic role of relative hyperinsulinemia. *Diabetes* 49, 2094–2101.
- Yoon, K.H., Ko, S.H., Cho, J.H., Lee, J.M., Ahn, Y.B., Song, K.H., Yoo, S.J., Kang, M.I., Cha, B.Y., Lee, K.W., et al. (2003). Selective beta-cell loss and alpha-cell expansion in patients with type 2 diabetes mellitus in Korea. *J. Clin. Endocrinol. Metab.* 88, 2300–2308.

STAR★METHODS

KEY RESOURCES TABLE

REAGENT or RESOURCE	SOURCE	IDENTIFIER
Antibodies		
Guinea-pig polyclonal anti insulin	Dako	Cat# A-0546; RRID:AB_10013624
Mouse monoclonal anti glucagon	Sigma	Cat# G2654; RRID:AB_259852
Rat polyclonal anti somatostatin	Abcam	Cat# ab30788; RRID:AB_778010
Goat anti-guinea-pig Secondary Antibody Alexa Fluor 488	Thermo Fisher Scientific	Cat# A-11073; RRID:AB_2534117
Goat anti-rat Secondary Antibody Alexa Fluor 546	Thermo Fisher Scientific	Cat# A-11081; RRID:AB_141738
Goat anti-mouse Secondary Antibody Alexa Fluor 633	Thermo Fisher Scientific	Cat# A-21050; RRID:AB_141431
Biological Samples		
Human tissue	University Clinic Carl Gustav Carus, Dresden	N/A
Chemicals, Peptides, and Recombinant Proteins		
Aprotinin	Sigma	Cat# A6106
DAPI	Sigma Aldrich	Cat# D9542
Fluorescein diacetate	Sigma	Cat# F7378
Low melting point agarose	Carl Roth	Cat# 6351.1
Propidium iodide	Life Technologies	Cat# P1304MP
Critical Commercial Assays		
Insulin Ultra Sensitive Assay HTRF Kit	Cisbio	Cat# 62IN2PEH
Software and Algorithms		
GraphPad PRISM 6.01	GraphPad Software, La Jolla, California, USA	http://www.graphpad.com
Fiji	Schindelin et al., 2012	https://fiji.sc/
MorphoLibJ	Legland et al., 2016	https://imagej.net/MorphoLibJ
Other		
Perfusion System	Biorep Technologies, USA	Cat# PERI4-02-230-FA
Semiautomatec vibratome VT1200S	Leica	Cat# 14048142066
LSM780 NLO Confocal microscope	Zeiss	N/A
Closed perfusion chamber + platform	Warner Instruments	Cat# 64-0223 and 64-0281

LEAD CONTACT AND MATERIALS AVAILABILITY

This study did not generate new unique reagents. Further information and requests for resources and reagents should be directed to and will be fulfilled by the Lead Contact, Stephan Speier (stephan.speier@tu-dresden.de).

EXPERIMENTAL MODEL AND SUBJECT DETAILS

The here presented study was approved by the local ethics committee ("Ethik-Kommission der Medizinischen Fakultät Carl Gustav Carus der Technischen Universität Dresden"). Written informed consent was received from all participants prior to inclusion in the study. Human pancreatic tissue was obtained through a collaboration between the Paul Langerhans Institute Dresden and the University Clinic Carl Gustav Carus which was initiated as part of the IMI IMIDIA consortium ([Solimena et al., 2018](#)) and continued in the IMI RHAPSODY and INNODIA consortia. Patients undergoing partial pancreatectomy were thoroughly metabolically phenotyped prior to surgery and classified into groups of non-diabetic (ND, n = 4), impaired glucose tolerant (IGT, n = 4) and type 2 diabetic (T2D, n = 6). Age/sex and metabolic parameters were provided for all patients ([Table S1](#))

METHOD DETAILS

Tissue Procurement, Processing and Slicing

Within 1.5 hours after explant, surgical tissue specimens were placed into ECS solution (125mM NaCl, 2.5mM KCl, 26mM NaHCO₃, 1.25mM NaH₂PO₄, 1mM MgCl₂, 2mM CaCl₂, 10mM HEPES, 3mM glucose, pH 7.4) and processed into smaller tissue blocks by removing connective, adipose and fibrotic tissue. Up to four small tissue pieces of ca. 3x3x3mm were placed into a 3.5cm Petri dish and covered with 3.8% low melting point agarose (Carl Roth, 6351.1) preheated to 37°C. Once agarose was solidified, the small agarose cubes containing tissue blocks were mounted using tissue glue (Superglue 90-120 CPS, World Precision Instruments, Inc, cat. no. 7341) on the specimen holder of a semiautomatic vibratome (Leica VT1200S, cat. no. 14048142066) and the buffer tray was filled with cold ECS solution. Slicing was performed at a step size of 120 µm, speed of 0.1mm/s, amplitude of 1mm and an angle of 15°. Slices were collected into a 6cm Petri dish containing 3mM glucose KRBH buffer (137mM NaCl, 5.36mM KCl, 0.34mM Na₂HPO₄, 0.81mM MgSO₄, 4.17mM NaHCO₃, 1.26mM CaCl₂, 0.44mM KH₂PO₄, 10mM HEPES, 0.1% BSA, 3mM glucose, pH 7.3) with aprotinin (25KIU/mL, Sigma, cat. no. A6106) and kept for 60 minutes at room temperature while shaking, before performing any further experiments.

Tissue Viability

Tissue viability was assessed after slicing using FDA/PI staining. Two slices of each embedded block were incubated with propidium iodide staining solution (f. c. 0.1mg/mL in PBS, Life technologies, cat. no. P1304MP-100mg) for 1-2 minutes at room temperature while shaking. Fluorescein diacetate (f.c. 0.05mg/mL in PBS, Sigma, cat. no. F7378-5g) was added to the staining solution and incubated for 2 minutes at room temperature in the dark, while shaking. Slices were transferred into PBS (Sigma, cat. no. D8537-500ml) and imaged using a confocal microscope (LSM 780 NLO, Zeiss). If propidium iodide positive cells within the tissue (excluding the cutting surface) exceeded ~10%, we excluded the patient from the study.

Perfusion

Four slices originating from different embedded blocks were placed into a closed perfusion chamber (Warner Instruments, cat. no. 64-0223 and cat. no. 64-0281 (P-5)) and connected to a perfusion system with automated tray handling (Biorep Technologies, cat. no. PERI4-02-230-FA). In order to equilibrate the slices to 37°C and to wash out accumulated hormones and enzymes from the tissue, a 60-minute flushing step with 3mM KRBH at a flow rate of 100 µL/min was performed. Subsequently, the actual perfusion protocol was applied using a flow rate of 100µL/min and samples were collected in 96-well plates containing aprotinin at a final concentration of 25 KIU/mL at an interval of 2 minutes. After the perfusion experiments, tissue slices were lysed for total insulin content measurements using 500 µL acid ethanol (2% HCl [37%, 12M] in abs. ethanol). Samples were kept at -20°C until measured with an Insulin Ultra Sensitive Assay Kit (Cisbio, cat. no. 62IN2PEH).

Immunofluorescent staining

Slices were fixed with 4% paraformaldehyde for 30 minutes at room temperature and kept in PBS at 4°C until staining. All antibody solutions were prepared in staining buffer containing 30% goat serum, 900mM NaCl, 40mM sodium phosphate buffer (pH 7.4) and 0.6% Triton X-100. Slices were incubated with primary antibodies against insulin (1:500, guinea-pig, Dako, cat. no. A-0546), glucagon (1:2000, mouse, Sigma, cat. no. G2654) and somatostatin (1:200, rat, Abcam, cat. no. ab30788) overnight at 4°C while shaking. Slices were washed three times for at least 30 minutes with PBS and incubated with secondary antibodies: AlexaFluor® 488 goat anti-guinea-pig (1:200, Invitrogen, cat. no. A-11073), AlexaFluor® 633 goat anti-mouse (1:200, Invitrogen, cat. no. A-21050) AlexaFluor® 546 goat anti-rat (1:200, Invitrogen, cat. no. A-11081) and DAPI (2.5mg/ml, Sigma Aldrich, cat. no. D9542) overnight at 4°C while shaking. Slices were washed three times for at least 30 minutes with PBS and kept at 4°C in the dark until imaging.

Imaging and Analysis

Single islet images were obtained using an upright laser scanning confocal microscope (LSM 780 NLO, Zeiss) with a Plan-Apochromat 20x/1.0 water-immersion objective (Zeiss) using a stack separation of 1.5 µm. For the assessment of 2D islet morphology, 10-20 islets per patient were imaged from at least 3 different slices and analysis was performed manually on three z-planes per islet at a distance of 15 µm using Fiji (Schindelin et al., 2012). Islet cell composition was expressed as the average of the three planes analyzed. For imaging of entire tissue slices, tile-scans were performed with 2-4 stained slices per patient mounted under a poly-L-lysine coated 22x22mm glass coverslip submerged in PBS (pH 7.4) using an upright laser scanning confocal microscope (LSM 780 NLO, Zeiss), with a Plan-Apochromat 20x/1.0 water-immersion objective (Zeiss) and an automated stage (Zeiss). Single tiles were imaged at a resolution of 0.75x0.75µm, a tile overlap of 15%, and stack separation of 2.5µm. The bounding grid was set around the slice such that the entire slice was included in the tile-scan, and the stack boundaries were set to include the entire slice.

Tile-Scan Analysis

Raw tile-scans were stitched using the Fiji Stitching plugin (Preibisch et al., 2009; Schindelin et al., 2012). Fusion was completed by maximum intensity, with a regression threshold of 0.3, maximum displacement threshold of 2.50, and absolute displacement threshold of 3.50. The overlap was computed with sub pixel accuracy. Stitched tile-scans were contoured manually for the total slice

area and for all individual endocrine objects (defined as positive for at least one hormone stained) on a maximum intensity projection, with the ROIs saved separately. For individual endocrine objects, the regions were individually cropped from the stitched tile-scan, the 488 channel was subtracted from the 546 channel, and the 546 channel was subtracted from the 633 channel to account for channel bleed. The images were then split by color, median filtered (3x3x1), and each converted to binary (IJ_IsoData). Hole filling in 3D and size opening (limit 500 μm^3), followed by volume analysis (Euler connectivity: C26) were completed using MorphoLibJ (Legland et al., 2016). For total slice volume, each channel of the original tile-scan was added together, and then cropped using the total slice ROI previously contoured. The image was median filtered (3x3x1), and a mask of nearby points was generated (within a distance of 10.0 μm , threshold of 12.75) using the built in Fiji plugin. Dark and bright outliers (respectively) with a radius of 20 pixels each were removed. Holes were filled, 3D volume closing was run (cube, 3x3x1), and volume analysis was completed as for the endocrine objects using MorphoLibJ (Legland et al., 2016). Analyzed volumes and endocrine object counts were pooled by patient number for the purposes of statistical analysis. For further analysis, endocrine objects were grouped by volume into single cells (500 – 1,000 μm^3), small endocrine clusters (1,001 – 10,000 μm^3 , corresponding volume for 2–10 cells) and islets (> 10,000 μm^3 , corresponding volume of 11 or more cells). Comparing endocrine cell composition of similar sized islets assessed by volumetric 3D morphometry of entire tissue slices and manual 2D analysis of single image sections of an islet, we verified that semi-automated large-scale 3D morphometry delivers the same precision as conventional manual cell counting in 2D, while providing a much larger amount of data with more specific and relevant information about pancreas morphology (Figure S6).

QUANTIFICATION AND STATISTICAL ANALYSIS

Statistical Analyses and Calculations

No specific statistical methods were used to predetermine sample size. All results are presented as mean \pm SEM. The significance of the difference between groups was analyzed as described in the figure legends. P values < 0.05 were considered statistically significant. All statistical analyses were performed using GraphPad Prism Software version 6.01.

DATA AND CODE AVAILABILITY

This study did not generate any unique datasets or code

Supplemental Information

**Dysfunction of Persisting β Cells Is a Key
Feature of Early Type 2 Diabetes Pathogenesis**

Christian M. Cohrs, Julia K. Panzer, Denise M. Drotar, Stephen J. Enos, Nicole Kipke, Chunguang Chen, Robert Bozsak, Eyke Schöniger, Florian Ehehalt, Marius Distler, Ana Brennand, Stefan R. Bornstein, Jürgen Weitz, Michele Solimena, and Stephan Speier

SUPPLEMENTAL MATERIAL

Dysfunction of Persisting β -Cells is a Key Feature of Early Type 2 Diabetes Pathogenesis

Christian M. Cohrs^{1,2,3,9}, Julia K. Panzer^{1,2,3,9}, Denise M. Drotar^{1,2,3}, Stephen J. Enos^{1,2,3}, Nicole Kipke^{3,4}, Chunguang Chen^{1,2,3}, Robert Bozsak^{1,2,3}, Eyke Schöninger^{1,3,4}, Florian Ehehalt⁵, Marius Distler⁵, Ana Brennand⁶, Stefan R. Bornstein^{6,7}, Jürgen Weitz^{1,5}, Michele Solimena^{1,3,4,8}, and Stephan Speier^{1,2,3*}

¹Paul Langerhans Institute Dresden (PLID) of the Helmholtz Zentrum München at the University Clinic Carl Gustav Carus of Technische Universität Dresden, Helmholtz Zentrum München, Neuherberg, Germany.

²Institute of Physiology, Faculty of Medicine, Technische Universität Dresden, Germany.

³German Center for Diabetes Research (DZD), München-Neuherberg, Germany.

⁴Molecular Diabetology, Faculty of Medicine, Technische Universität Dresden, Germany.

⁵Department of GI-, Thoracic- and Vascular Surgery, University Hospital Carl Gustav Carus, Technische Universität Dresden, Germany.

⁶Department of Diabetes, School of Life Science & Medicine, Faculty of Life Sciences & Medicine, King's College London, London, United Kingdom.

⁷Department of Medicine III, University Hospital Carl Gustav Carus, Dresden, Germany.

⁸Max Planck Institute of Molecular Cell Biology and Genetics, Dresden Germany.

⁹These authors contributed equally to this work.

No.	gender	age	BMI	diabetic status	tumor type	surgical method	pancreas region	diabetes duration (yrs)	medication	insulin supplement	HbA1c (%)	fasting BG (mmol/L)	2h BG during oGTT (mmol/L)	fasting insulin (pmol/L)	fasting C-peptide (nmol/L)	fasting proinsulin (pmol/L)	insulin : proinsulin ratio	HOMA2-IR	HOMA2-%B
1	M	69	31.2	ND	pseudocyst	PL	tail	-	-	-	5.1	5.76	7.20	110	1.16	1.8	61.11	2.67	140.00
2	M	64	24.4	ND	adenocarcinoma	PPPD	head	-	-	-	4.8	5.29	6.75	120	1.27	2.7	44.44	2.84	174.90
3	M	62	24.7	ND	adenocarcinoma	PPPD	head	-	-	-	5	4.73	5.50	30	0.41	1.7	17.65	0.89	98.90
4	M	52	32	ND	metastasis renal cancer	PL	tail	-	-	-	5.3	5.84	5.50	60	0.59	1.5	40.00	1.37	84.50
5	F	72	39.4	IGT	pancreatic dysplasia	total pancreatectomy	tail	-	-	-	5.3	5.98	9.54	170	1.74	1.5	113.33	4.03	175.70
6	M	67	22.4	IGT	adenocarcinoma	Whipple	head	-	-	-	4.9	5.49	10.35	70	1.14	2.8	25.00	2.58	151.10
7	M	67	31.7	IGT	IPMN	PPPD	head	-	-	-	5.2	5.30	8.97	30	0.46	1.6	18.75	1.03	85.70
8	F	79	28.1	IGT	adeno-neuroendocrine carcinoma	PPPD	head	-	-	-	5.8	4.90	10.91	90	1.28	2.8	32.14	2.79	203.00
9	M	74	36.0	T2D	IPMN	Whipple	head	15	-	X	7.4	14.00	-	50	0.66	2.2	22.73	2.16	20.30
10	M	76	31.8	T2D	solitary fibrous tumor	PPPD	head	17	Metformin	X	6.6	9.45	-	40	0.81	1.4	28.57	2.18	44.60
11	F	63	22.8	T2D	adenocarcinoma	total pancreatectomy	head	3	diet	-	7.2	7.72	-	90	0.96	3.7	24.32	2.42	71.90
12	F	80	23.3	T2D	adenocarcinoma	total pancreatectomy	head	10	Metformin	X	7.3	9.02	-	30	0.95	3.1	9.68	2.52	54.50
13	F	66	27.8	T2D	adenocarcinoma	PPPD	head	20	EMPA, Metformin	-	7.7	10.11	-	30	0.87	4.4	6.82	2.40	42.10
14	F	71	34.9	T2D	carcinoma of distal bile duct	total pancreatectomy	head	6	SGLT-2i, Metformin	X	6.7	9.61	-	30	0.52	3.3	9.09	1.41	30.90

Table S1: Related to Figure 1. Clinical parameters of donor patient used for tissue slice study

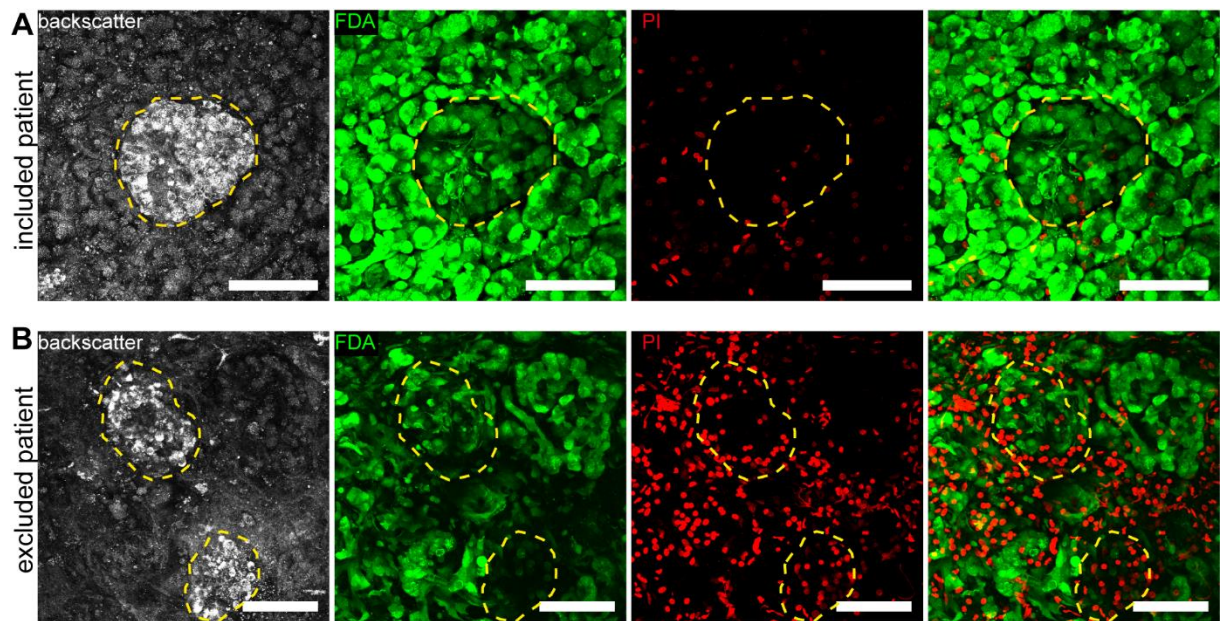


Figure S1. Viability assessment of human pancreas tissue slices. Related to STAR methods. Maximum intensity projections of the slice backscatter light signal (grey), FDA (green) and PI (red) as well as the merged FDA/PI signal from *A*: viable slices included in the study and *B*: from primarily dead slices where tissue of the respective patient was excluded for subsequent assays. Scale bar, 100 μm .

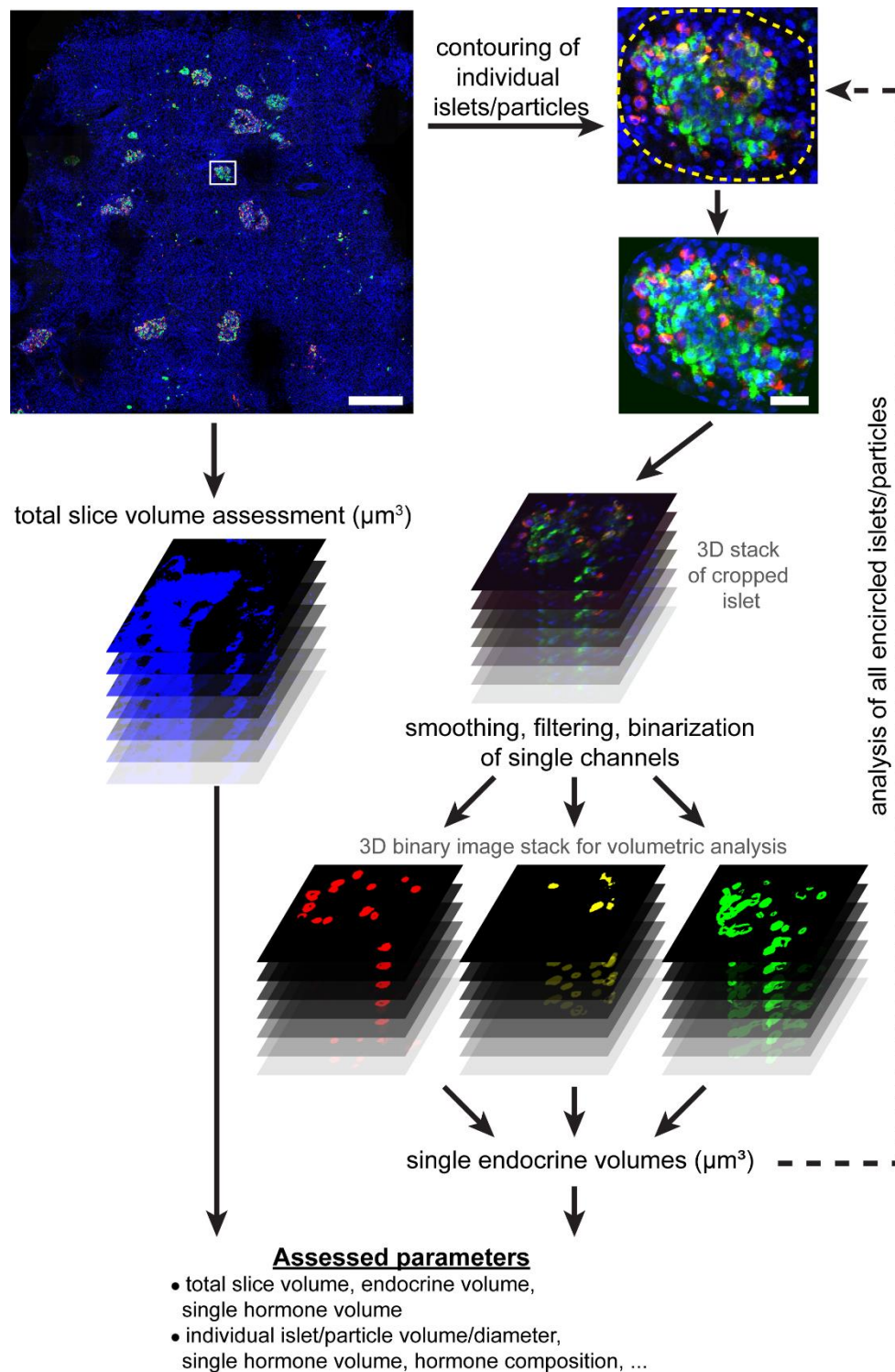


Figure S2. Analysis pipeline for 3D histomorphometry. Related to Figure 2. The maximum intensity projection of a stitched whole tissue slice scan will be used to contour all individual endocrine objects. These regions are then cropped out and the entire z-stack (from the original file) will be used for pre-processing (smoothing, filtering and binarization) of the single channels and then subjected to volumetric analysis to resulting in individual endocrine volumes that can be used for further analyses. In addition, the whole tissue volume of the slice is assessed volumetrically (using all fluorophores imaged). Scale bars = 500 μm (overview image), 30 μm (single islet image)

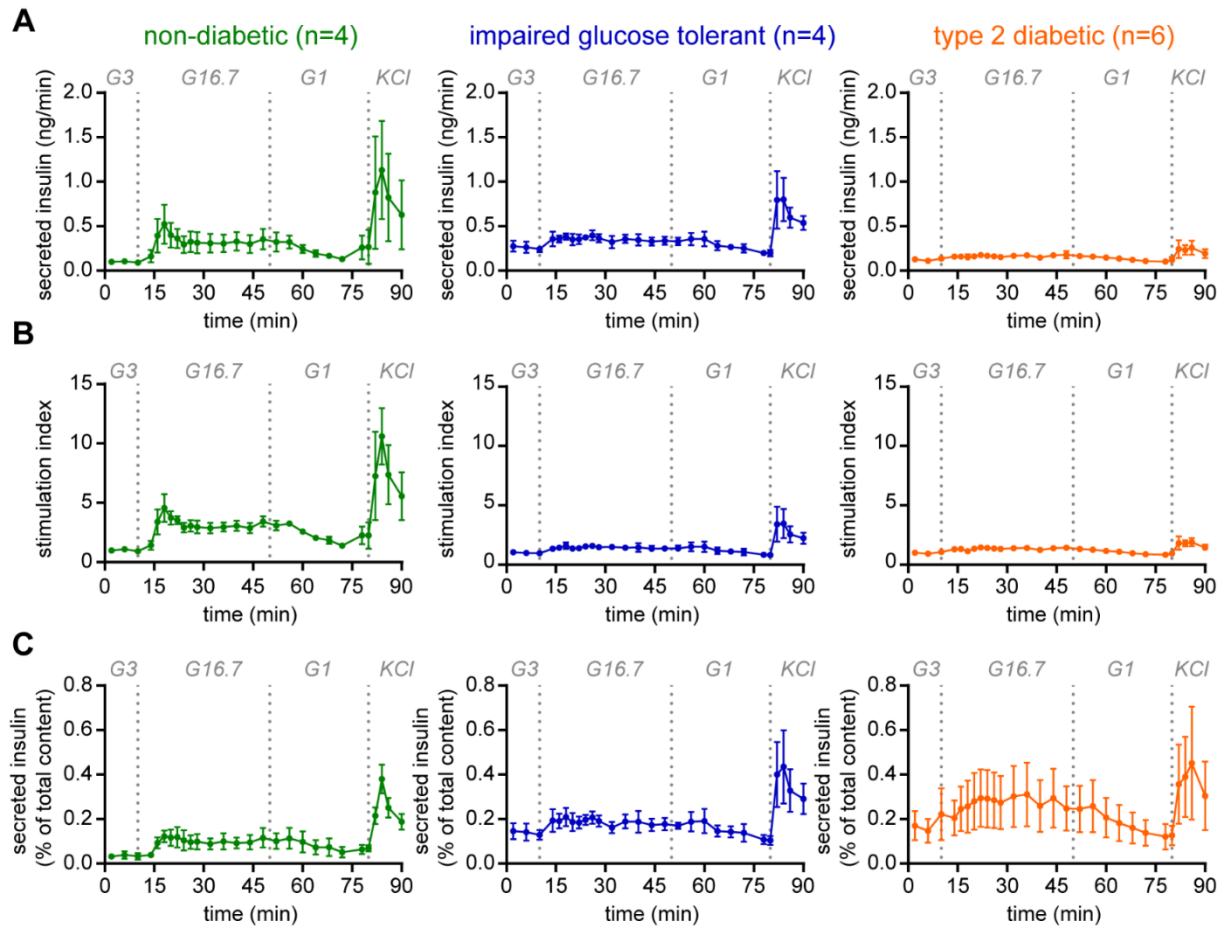


Figure S3. Separate traces of insulin secretory pattern. Related to Figure 3. Separate traces of ND (green), IGT (blue) and T2D (orange) pancreas tissue slices expressed as *A*: as absolute secretion in ng/min, *B*: fold increase to basal secretion within the first 10 minutes and *C*: % of total content. G3 = KRBH buffer containing 3mM glucose, G16.7mM = KRBH buffer with 16.7mM glucose, G1 = KRBH buffer containing 1mM glucose, KCl = KRBH buffer with 16.7mM glucose and 60mM KCl (f.c.). ND n=4, IGT n=4, T2D n=6 with data presented as mean \pm SEM.

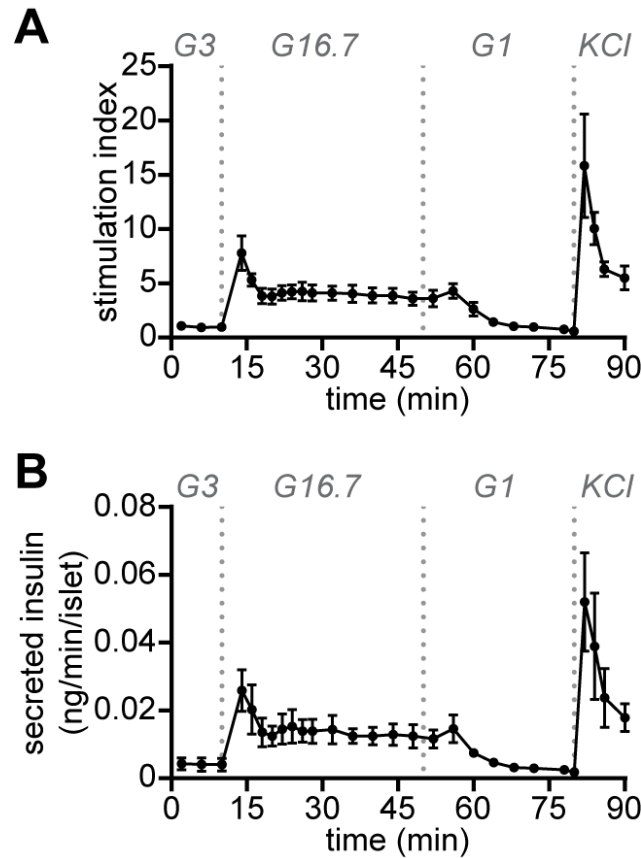


Figure S4. β -cell function in isolated human islets. Related to Figure 3. Insulin secretory pattern during perfusion of isolated human islets provided by King's College London after shipment and overnight rest from ND donors ($n=4$) expressed as A: fold increase to basal secretion within the first 10 minutes (3mM glucose) and B: as absolute secreted insulin per minute for one islet. G3 = KRBH buffer containing 3mM glucose, G16.7 = KRBH buffer with 16.7mM glucose, G1 = KRBH buffer containing 1mM glucose, KCl = KRBH buffer with 16.7mM glucose and 60mM KCl (f.c.). Data is presented as mean \pm SEM. Donor information: male, age: 24-49 years, BMI: 23.55 – 34.02

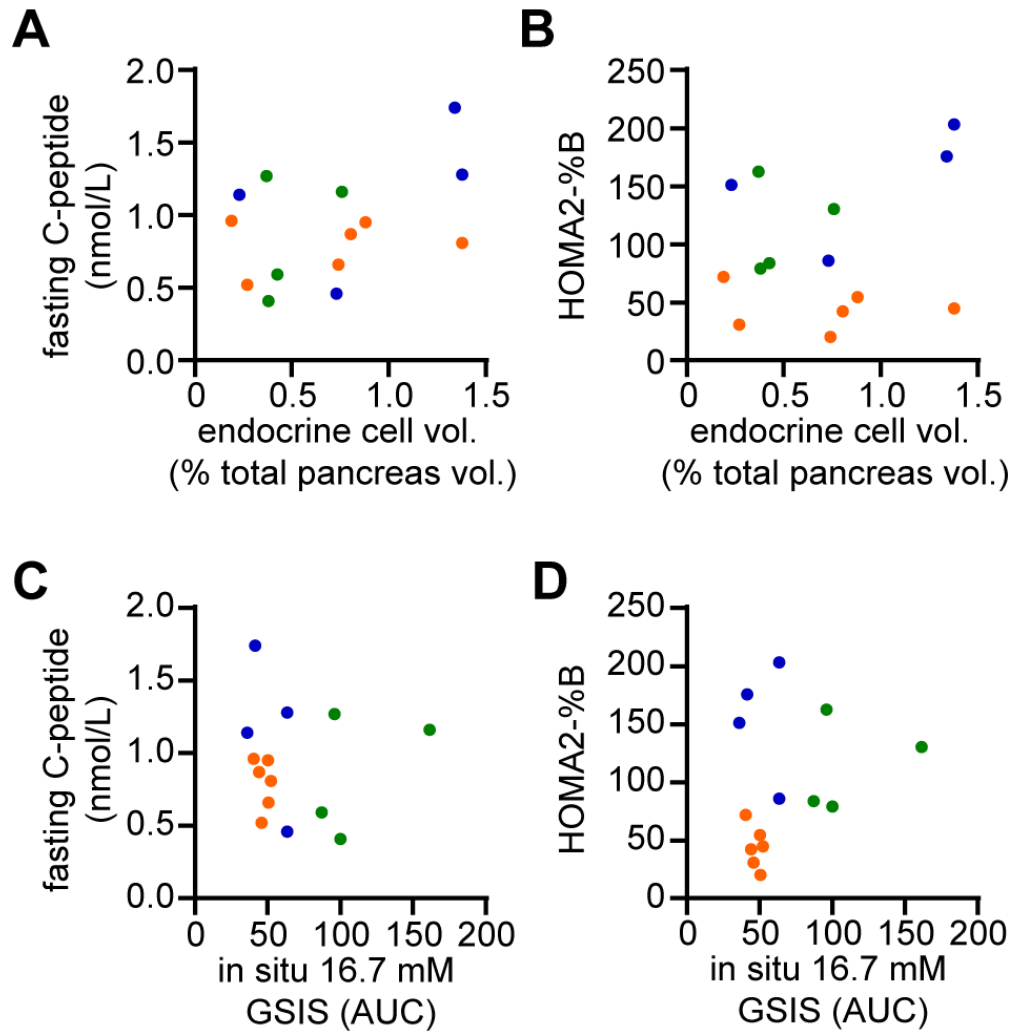


Figure S5. Association of clinical parameters with β -cell function and mass. Related to Figure 4. *A-B*: Correlation of endocrine cell volume (see Fig. 2D) with *A*: fasting C-peptide and *B*: HOMA2-%B. *C-D*: Correlation of AUC values from insulin secretion (stimulation index) during stimulating conditions with 16.7mM glucose (see Fig. 3) with *C*: fasting C-peptide and *D*: HOMA2-%B. ND (green) $n=4$, IGT (blue) $n=4$, T2D (orange) $n=6$.

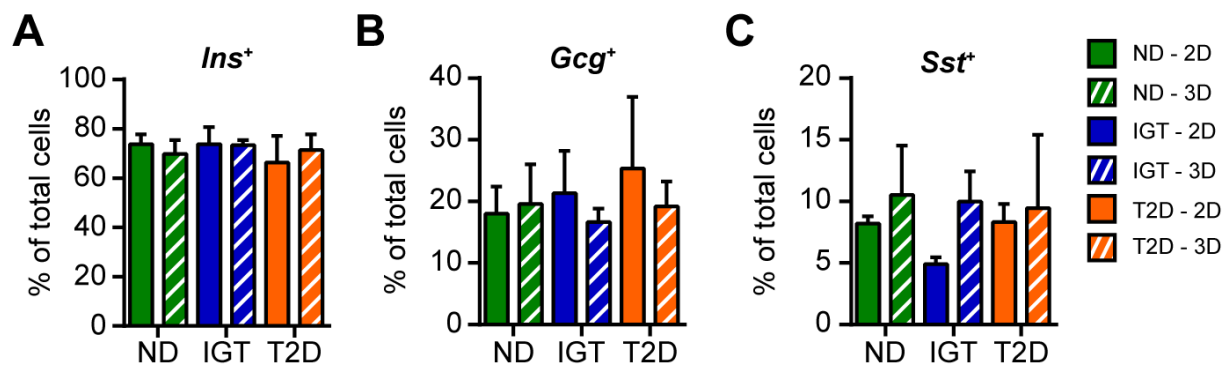


Figure S6. Comparison of 2D and 3D islet morphometry. Related to STAR methods. A-C: Total endocrine cell fraction for A: insulin⁺, B: glucagon⁺ and C: somatostatin⁺ cells separated by disease type and analysis method. 2D analysis was conducted by manual counting of 3 individual planes within a stack with at least 15 μm separation (2D). A total of 10-20 islets per patient were analyzed with islet diameter ranging between 35 and 265 μm . For islet compositional analysis from the automated whole slice 3D analysis an islet size threshold of >35 μm was used to be comparable to the manual 2D analysis. ND n=3, IGT n=4, T2D n=5 with data presented as mean \pm SEM; statistical analysis was performed between 2D and 3D values by unpaired two-tailed t-tests at 95% CI.